DOI: 10.1002/ejic.200900203

Generation and Properties of Co^{I}/Ni^{I} Species Stabilized by a Tetradentate Pyridylpyrazole Ligand: Crystal Structures of Dialkyl-Co^{III} Complexes

Vibha Mishra,[a] Haritosh Mishra,[a] and Rabindranath Mukherjee*[a]

Keywords: Cobalt / Nickel / Redox chemistry / EPR spectroscopy / Nitrogen heterocycles / N ligands / Chelates

Mononuclear Co^{II} and Ni^{II} complexes $[(L^1)Co^{II}(H_2O)_2][ClO_4]_2$ (**1**) and $[(L^1)Ni^{II}(MeCN)_2][BPh_4]_2$ (**3**) (L^1 = 2,2′-[propane-1,3-diylbis(1*H*-pyrazole-1,3-diyl)]dipyridine) display a quasireversible M^{II}/M^{I} redox process ($E_{1/2}$ = –0.96 V vs. SCE, ΔE_p = 110 mV for **1**; $E_{1/2}$ = –0.71 V vs. SCE, ΔE_p = 90 mV for **3**). The dinuclear Co^{II} complex $[(L^1)_2Co^{II}_2(\mu\text{-}O_2CMe)_2][BPh_4]_2$ (**2**) displays a quasireversible reductive response ($E_{1/2}$ = –1.46 V vs. SCE, ΔE_p = 120 mV), supposedly due to Co^{II}_2/Co^{I}_2 redox process. For these complexes chemical ($NaBH_4$) and electrochemical reduction generate Co^{I} and Ni^{I} species. The existence of dark purple Ni^{I} species has been authenticated by its UV/Vis spectral feature (crystal-field transition at 901 nm and metal-to-ligand charge-transfer transition at 537 nm) and axial EPR spectrum ($g_{\parallel}$ = 2.27 and $g_{\perp}$ = 2.08). Dark greenish blue/bright green Co^{I} species were characterized by absorption spectroscopy. Reaction of chemically generated Co^{I} species with CH_3I resulted in the formation of dimethyl-Co^{III} complexes. Notably, Co^{I} species generated from monomeric complex **1** led to the formation of two products: a mononuclear complex $[(L^1)Co^{III}(CH_3)_2][ClO_4]$ (**4**) (minor) and a dinuclear complex $[(L^1)_2Co^{III}_2(CH_3)_4][ClO_4]_2$ (**5**) (major). In contrast, when the dimeric complex **2** was reduced with $NaBH_4$ and reacted with CH_3I the monomeric complex $[(L^1)Co^{III}(CH_3)_2][BPh_4]$ (**6**) was isolated in reasonable yield. All three organometallic dialkyl-Co^{III} complexes **4**–**6** have been characterized by elemental analysis, ^1H NMR spectroscopy, and X-ray crystallography.

Introduction

In coordination chemistry research judicious choice of a ligand system incorporating specific electronic and stereochemical (conformational rigidity/flexibility) feature plays a crucial role in the stabilization of a metal oxidation state.[1] The stereochemical flexibility of a ligand providing facile structural adjustment between differing coordination geometry dictated by redox interconversion (for example, octahedral to square planar for d^7 Co^{II} to d^8 Co^{I} and octahedral to square-based geometry for d^8 Ni^{II} to d^9 Ni^{I}) is important to stabilize metal ions in lower oxidation states. It has been well-documented that a flexible ligand augments stabilization of Ni^{I} species.[2–6]

The key feature of nitrogen heterocycles[7–10] containing six-membered rings (e.g. 2,2′-bipyridine and 1,10-phenanthroline) is their low-lying π*-antibonding orbitals which make them excellent π acceptors; consequently they have been used to stabilize various metal ions in lower oxidation states. On the other hand, five-membered ring heterocyles (e.g. pyrazole) are much poorer π acceptors (and better π donors). Notably, the ligand of pertinence to this work 2,2′-[propane-1,3-diylbis(1*H*-pyrazole-1,3-diyl)]dipyridine (L^1) contains both soft (pyridine) and hard (pyrazole) donor sites. As a part of our activity in exploring metal-binding properties of pyridylpyrazole ligands[10–13] we have recently reported[14] the coordination chemistry of the tetradentate ligand L^1,[15] towards mononuclear Co^{II} and Ni^{II}. Moreover, we have addressed the issue of stereoelectronic preference of Ni^{II} and Cu^{II} ions[16] to assume five-/six-coordinate geometry in their binuclear complexes and stabilized the mixed-valence Ni^{III}–Ni^{II} species [from coulometric oxidation of structurally characterized complex $[\{(L^2)Ni^{II}\}_2(\mu\text{-}pypz)_2][ClO_4]_2$, supported by a potentially tridentate ligand 2-[1-(pyridin-2-ylmethyl)-1*H*-pyrazol-3-yl]pyridine (L^2)[12d] as terminal and 3-(2-pyridyl)pyrazolate ion (pypz anion)[17,18] as bridging ligand]. The ligand L^1 is unique in the sense that it has two bidentate pyridyl–pyrazolyl fragments linked by a flexible –CH_2–CH_2–CH_2– spacer, which can either coordinate to a single metal ion as a tetradentate chelate as in the complexes $[Fe^{II}(L^1)(DMF)_2][ClO_4]_2$, $[Cu^{II}(L^1)][BF_4]_2$, $[Ag(L^1)][NO_3]\cdot CH_3CN$, $[Ag(L^1)][ClO_4]$, $[Pb(L^1)(NO_3)_2]$, $[\{Zn(L^1)\}_3(\mu\text{-}OCO_2)][ClO_4]_4\cdot 3.5H_2O$, $[Co^{II}(L^1)(H_2O)_2][ClO_4]_2$, $[Ni^{II}(L^1)(MeCN)_2][BPh_4]_2$, and $[Ni^{II}(L^1)(O_2CMe)][BPh_4]$[14,15] or can coordinate each bidentate arm to a separate metal center to give bridged binuclear/polynuclear species as in the binuclear complex $[Co^{II}_2(L^1)_2(\mu\text{-}O_2CMe)_2][BPh_4]_2$.[14] Thus the competition between bridging and chelating coordination modes of L^1 is an important factor in determining the course of a chemical reaction.

[a] Department of Chemistry, Indian Institute of Technology Kanpur,
Kanpur 208016, India
Fax: +91-512-2597437
E-mail: rnm@iitk.ac.in

Supporting information for this article is available on the WWW under http://dx.doi.org/10.1002/ejic.200900203.

The purpose of this study is threefold. First, to examine whether or not the ligand L^1 is capable of stabilizing Co^I/Ni^I oxidation state as a result of reduction of their Co^{II}/Ni^{II} complexes $[Co^{II}(L)(H_2O)_2][ClO_4]_2$ (**1**), $[Co^{II}_2(L)_2(\mu\text{-}O_2CMe)_2][BPh_4]_2$ (**2**), and $[Ni^{II}(L)(MeCN)_2][BPh_4]_2$ (**3**). Secondly, if accessible, to investigate the reaction between the Co^I species and CH_3I to generate/isolate Co^{III}–CH_3 complexes.[19–22] From this perspective herein we report redox properties of complexes **1**–**3**, which reveal the possibility of stabilizing Co^I/Ni^I species by L^1. This report also deals with spectroscopic characterization of Co^I/Ni^I species and the reactions of chemically generated Co^I species with CH_3I. We present ^1H spectroscopic and X-ray crystallographic characterization of three Co^{III}–CH_3 complexes $[Co^{III}(L^1)(CH_3)_2][ClO_4]$ (**4**), $[Co^{III}_2(L^1)_2(CH_3)_4][ClO_4]_2$ (**5**), and $[Co^{III}(L^1)(CH_3)_2][BPh_4]$ (**6**).

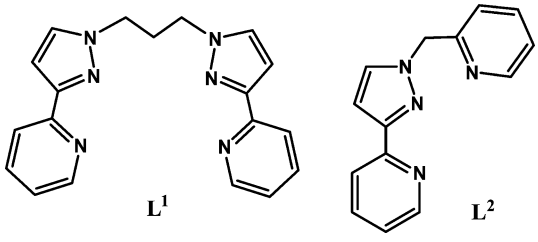

Results and Discussion

Electrochemical Generation and Characterization of Co^I and Ni^I Species

The redox behavior of structurally characterized complexes $[Co^{II}(L^1)(H_2O)_2][ClO_4]_2$ (**1**), $[Co^{II}_2(L^1)_2(\mu\text{-}O_2CCH_3)_2][BPh_4]_2$ (**2**), and $[(L^1)Ni^{II}(CH_3CN)_2][BPh_4]_2$ (**3**) have been investigated by cyclic voltammetry (CV) in CH_3CN at a platinum electrode (scan rate = 100 mV s^{-1}). Complex **1** exhibits a quasireversible response with $E_{1/2}$ = –0.96 V vs. SCE (ΔE_p = 110 mV) which is assigned to Co^{II}/Co^I redox process (Figure 1). Two broad humps due to ligand-centered reductions could also be seen at –1.70 V and –2.06 V. Controlled-potential electrolysis of complex **1** at –1.10 V vs. SCE led to the reduction of the Co^{II} center (n = 0.88 ± 0.04) with concomitant change of color from light pink to greenish-blue. The greenish-blue Co^I solutions exhibit an irreversible oxidative response at –0.90 V vs. SCE, implying rapid decomposition of the reduced solutions. Greenish-blue solutions, generated by chemical reduction with $NaBH_4$, behave in an identical manner. Although electrochemically generated Co^I species was found quite unstable, the absorption spectra of such solutions (Figure 2) were recorded. A very broad band centered at λ = 656 nm with $\varepsilon \approx 1000$ M^{-1} cm^{-1} was observed, which is assigned to metal-to-ligand charge-transfer transition.

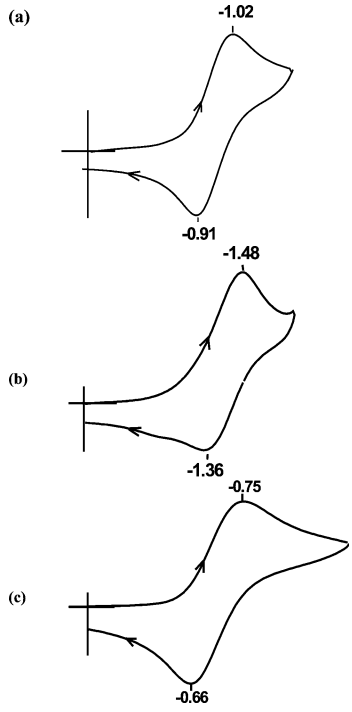

Figure 1. Cyclic voltammograms (scan rate = 100 mV s^{-1}) of (a) $[(L^1)Co^{II}(H_2O)_2][ClO_4]_2$ (**1**), (b) $[(L^1)_2Co^{II}_2(\mu\text{-}O_2CMe)_2][BPh_4]_2$ (**2**), and (c) $[(L^1)Ni^{II}(CH_3CN)_2][BPh_4]_2$ (**3**) at a Pt electrode in CH_3CN (ca. 0.1 M in TBAP). Indicated potentials (in V) are vs. SCE.

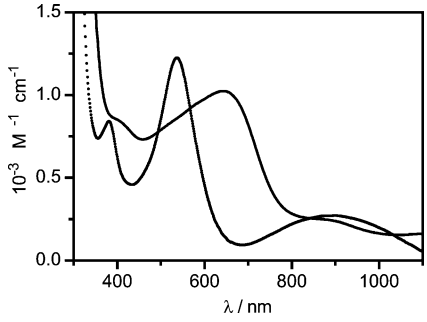

Figure 2. UV/Vis spectra in the range 300–1100 nm (in CH_3CN) of electrochemically generated solutions of $[(L^1)Co^{II}(H_2O)_2][ClO_4]_2$ (**1**) (solid line) and $[(L^1)Ni^{II}(CH_3CN)_2][BPh_4]_2$ (**3**) (line with symbol).

Complex **2** exhibits a quasireversible reductive response with $E_{1/2}$ = –1.46 V (ΔE_p = 120 mV) (Figure 1) and an additional irreversible reductive response at E_{pc} (cathodic peak potential) = –1.73 V vs. SCE. We assign the less cathodic response as due to Co^{II}_2/Co^I_2 redox process. More cathodic response is expected to be due to ligand-centered reduction. Bulk electrolysis at –1.66 V vs. SCE led to the reduction of the Co^{II} species (n = 1.88 ± 0.12) with concomitant change of color from light-pink to bright green. Solutions of Co^I species display charge-transfer transitions as a shoulder at 400 nm and a peak at 656 nm. Crystal-field transition is observed at 895 nm.

The mononuclear Ni^{II} complex **3** exhibits a well-behaved quasireversible reductive response at $E_{1/2}$ = –0.71 V vs. SCE (ΔE_p = 90 mV) (Figure 1), with an additional irreversible re-

ductive response at –1.60 V. We assign the first reductive wave as due to Ni^{II}/Ni^{I} redox process and the more cathodic response as ligand-centered. Constant-potential electrolysis of complex **3** at –0.90 V vs. SCE led to the generation of a deep purple Ni^{I} species ($n = 1.04 \pm 0.06$). Such solutions display oxidative CV response at $E_{1/2}$ = –0.72 V vs. SCE (ΔE_p = 110 mV).

In essence, coulometric reductions associated with M^{II}/M^{I} (M = Co or Ni) species indicate that the Ni^{I} species is comparatively more stable (at least on the CV time scale) than Co^{I} species. However, we should mention here that all our attempts failed to isolate a nickel(I) compound, supported by L^1. Spectroscopic characterization of Ni^{I} species has been achieved and the results are reported here (see below).

Spectroscopic Characterization of Ni^{I} Species

The EPR spectrum (Figure 3) of purple reduced solutions of complex **3** is typical of a d^9 nickel(I) species: $g_{\|} = 2.27$ and $g_{\perp} = 2.08$.[5,6] Notably, the observed spectrum could well be compared with mononuclear copper(II) complex $[Cu^{II}(L^1)][BF_4]_2$ (unpaired electron in $d_{x^2-y^2}$ orbital) of this ligand ($g_{\|} = 2.261$ and $g_{\perp} = 2.058$).[15] Nickel(I) species was further characterized by absorption spectroscopy (Figure 2). The purple solution exhibits an intense band at 537 nm ($\varepsilon \approx 1200\ M^{-1}cm^{-1}$), which is assigned as due to metal-to-ligand charge-transfer transition. Low intensity band at 900 nm ($\varepsilon \approx 200\ M^{-1}cm^{-1}$) is assigned as d-d transition.

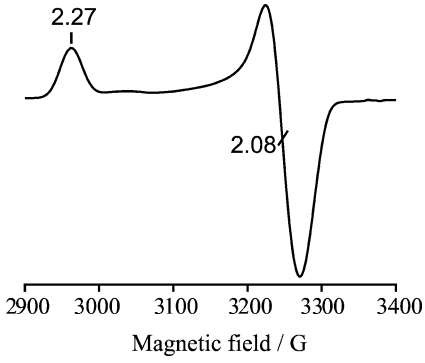

Figure 3. EPR spectrum (microwave frequency: 9.4485 GHz; microwave power: 0.201 mW; modulation amplitude: 10 G; modulation frequency: 100 kHz) at 120 K of dark purple Ni^{I} species obtained as a result of coulometric reduction of $[(L^1)Ni^{II}(CH_3CN)_2][BPh_4]_2$ (**3**) in CH_3CN.

Isolation and General Characterization of Co^{III}–$(CH_3)_2$ Complexes

Under a dinitrogen atmosphere and ice-cold conditions treatment of methanolic solutions of the complexes $[Co^{II}(L^1)(H_2O)_2][ClO_4]_2$ (**1**) and $[Co^{II}_2(L^1)_2(\mu\text{-}O_2CCH_3)_2][BPh_4]_2$ (**2**) with $NaBH_4$ generated Co^{I} species. Subsequent reactions of such solutons with CH_3I allowed to notice color change from pink to dark greenish blue/bright green to orange. Isolation of the complexes $[Co^{III}(L^1)(CH_3)_2][ClO_4]$ (**4**) (minor), $[Co^{III}_2(L^1)_2(CH_3)_4][ClO_4]_2$ (**5**) (major), and $[Co^{III}(L^1)(CH_3)_2][BPh_4]$ (**6**) were accomplished by following well-established procedures for oxidative addition reactions of highly nucleophilic monovalent cobalt complexes with alkyl halide.[20–22]

Complexes **4** and **6** are well-characterized by elemental analysis, UV/Vis, and ^1H NMR spectroscopy. Final characterization is achieved by their X-ray structural analysis. Complex **5** is, however, characterized by only X-ray crystallography, due to its poor solubility even in a highly polar solvent like DMSO.

Consistent with the presence of Co–C bond, dichloromethane solutions of comlexes **4** and **6** exhibit absorption spectral band in the 400–500 nm region [Figure S1 (Supporting Information)], due to $CH_3^- \rightarrow Co^{III}$ charge-transfer transition.[21,22]

Complexes **4** and **6** display ^1H NMR spectra between δ = 0–10 as expected for low-spin Co^{III} complexes [Figure S2 and Figure S3 (Supporting Information), respectively]. The proton resonances are assigned based on the available ^1H NMR spectral results for the free ligand L^1,[15] and for methyl-coordinated Co^{III} complexes.[19–22] Two singlets in the δ = 0.5–1.0 region are diagnostic of two methyl groups coordinated to metal ion.[19a] Chemical shifts for two methyl groups are not the same which can be understood from the X-ray structure of the complexes (see below). One methyl is coordinated to Co^{III} in *trans* position to pyridine nitrogen while the other one is trans to pyrazole nitrogen. The methylene hydrogen atoms of $–CH_2CH_2CH_2–$ spacer of the ligand L^1 are nonequivalent upon complexation and appeared as four multiplets between δ = 4–5.5 region; the presence of geminal and vicinal coupling within $–CH_2CH_2CH_2–$ unit makes a clearer interpretation difficult. The NMR signals of the aromatic protons of the 3-(2-pyridyl)pyrazole units are displayed in the region δ = 7.0–8.5. In essence, ^1H NMR result for complexes **4** and **6** clearly indicates that the solid-state structures (see below) are retained in solution.

Electrochemical Properties of Monomeric Dimethylcobalt(III) Complexes

When examined by CV (in CH_3CN at a platinum electrode, scan rate = 100 mV s^{-1}), the structurally characterized mononuclear dimethylcobalt(III) complexes $[(L^1)Co^{III}(CH_3)_2]X$ [X = ClO_4^- (**4**); X = BPh_4^- (**6**)] display two ill-defined reductive responses [Figures S4 and S5 (see Supporting Information), respectively], corresponding to the redox processes $[(L^1)Co^{III}(CH_3)_2]^+/[(L^1)Co^{II}(CH_3)_2]$ and $[(L^1)Co^{II}(CH_3)_2]/[(L^1)Co^{I}(CH_3)_2]^-$ at –1.46 V and –1.68 V (complex **4**) and –1.49 V and –1.73 V (complex **6**). Both the responses are irreversible, implying the occurrence of chemical reactions {dissociation of the alkyl group(s) from the reduced species $[(L^1)Co^{II}(CH_3)_2]$ and/or $[(L^1)Co^{I}(CH_3)_2]^-$} following electron-transfer reaction(s). Complex **6** displays an oxidative response at 0.77 V due to BPh_4^- oxidation.

Crystal Structures

In order to confirm the mode of coordination of the ligand L^1 and also to structurally authenticate the three complexes

4–**6** single-crystal X-ray structure determination was carried out. Selected bond lengths and angles are listed in Table 1.

Table 1. Selected bond lengths [Å] and angles [°] for $[(L^1)Co^{III}(CH_3)_2][ClO_4]$ (**4**), $[(L^1)_2Co^{III}_2(CH_3)_4][ClO_4]_2$ (**5**), and $[(L^1)Co^{III}(CH_3)_2][BPh_4]$ (**6**).

	4	**6**
Co–N(1)	2.064(6)	1.945(3)
Co–N(2)	1.951(6)	2.000(4)
Co–N(5)	2.062(5)	1.925(4)
Co–N(6)	1.942(6)	2.037(4)
Co–C(20)	1.974(7)	1.968(4)
Co–C(21)	1.989(6)	1.964(4)
N(1)–Co–N(2)	79.0(3)	81.07(2)
N(1)–Co–N(5)	97.3(2)	172.61(2)
N(1)–Co–N(6)	93.0(3)	96.40(2)
N(1)–Co–C(20)	171.4(3)	94.39(2)
N(1)–Co–C(21)	86.1(3)	86.81(2)
N(2)–Co–N(5)	92.1(2)	93.89(2)
N(2)–Co–N(6)	169.0(3)	98.09(2)
N(2)–Co–C(20)	100.8(3)	174.56(2)
N(2)–Co–C(21)	90.6(3)	91.14(2)
N(5)–Co–N(6)	81.3(3)	78.89(2)
N(5)–Co–C(20)	91.4(3)	90.91(2)
N(5)–Co–C(21)	176.0(3)	98.74(2)
N(6)–Co–C(20)	88.2(3)	85.34(2)
N(6)–Co–C(21)	96.4(3)	170.59(2)
C(20)–Co–C(21)	85.3(3)	85.6(2)
5[a]		
Co(1)–N(1)	2.192(12) [2.160(10)]	
Co(1)–N(2)	2.150(14) [2.175(11)]	
Co(1)–N(4)	2.147(12) [2.125(12)]	
Co(1)–N(5)	2.082(14) [2.156(12)]	
Co(1)–C(20)	2.028(9) [2.021(9)]	
Co(1)–C(21)	2.040(11) [2.034(9)]	
N(1)–Co(1)–N(2)	75.5(6) [76.0(4)]	
N(1)–Co(1)–N(4)	92.0(4) [91.1(4)]	
N(1)–Co(1)–N(5)	92.6(5) [92.2(4)]	
N(1)–Co(1)–C(20)	102.1(4) [105.2(4)]	
N(1)–Co(1)–C(21)	172.6(5) [174.7(5)]	
N(2)–Co(1)–N(4)	96.2(6) [96.8(5)]	
N(2)–Co(1)–N(5)	165.7(5) [166.7(4)]	
N(2)–Co(1)–C(20)	92.8(5) [93.4(4)]	
N(2)–Co(1)–C(21)	97.4(5) [99.0(4)]	
N(4)–Co(1)–N(5)	75.9(6) [77.1(5)]	
N(4)–Co(1)–C(20)	164.8(5) [162.5(4)]	
N(4)–Co(1)–C(21)	90.8(4) [91.2(4)]	
N(5)–Co(1)–C(20)	97.6(5) [95.6(5)]	
N(5)–Co(1)–C(21)	94.7(5) [93.0(4)]	
C(20)–Co(1)–C(21)	75.9(4) [73.1(4)]	

[a] Data for two molecules.

Structural Description of $[(L^1)Co^{III}(CH_3)_2][ClO_4]$ (4)

A view of the cationic part of complex **4** is depicted in Figure 4. The six-coordination around Co^{III} is provided by four nitrogen atoms [N(1), N(2), N(5), and N(6)] from the ligand L^1 coordinated in a *cis*-equatorial tetradentate chelating mode and by two methyl groups [C(20) and C(21)] *cis* to each other. It is interesting to note that in going from parent complex **1**,[14] to the dialkyl-Co^{III} complex **4** the ligand has changed its coordination mode from *trans* to *cis* tetradentate. This observation reflects the coordination flexibility of L^1, which is further realized in other two structures (see below). The two bidentate 3-(2-pyridyl)pyrazole units are not planar, the angle between the two CoN_2 planes is found to be 71.4°. The bond angles between *trans* atoms at the metal center are in the range 169.0(3)–176.0(3)° and the *cis* angles span wide ranges from 79.0(3)–100.8(3)°. Gross distortions from octahedral geometry are evident. The Co^{III}–N bond lengths are typical for low-spin Co^{III} complexes.[19–22] The Co^{III}–C bond lenghts [1.989(7) and 1.974(6) Å] are in the range reported for other Co^{III}–C complexes.[19–22]

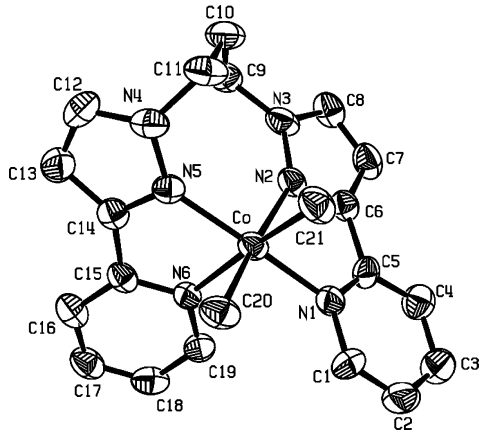

Figure 4. View of the cation $[(L^1)Co^{III}(CH_3)_2]^+$ in complex $[(L^1)Co^{III}(CH_3)_2][ClO_4]$ (**4**), showing the atom numbering scheme. All hydrogen atoms are excluded for clarity.

Synthetically prepared methylcobalt(III) complexes of N-donor ligands are invariably supported with tetrapyrroles, imines, oximes, mixed imine/oximes, or amines.[19e,19f] To the best of our knowledge, complexes **4**, **5**, and **6** (see below) are the first examples of structurally characterized dialkyl-Co^{III} complexes supported by nonmacrocyclic, conformationally flexible pyridylpyrazole-based tetradentate ligand.

Structural Description of $[(L^1)_2Co^{III}_2(CH_3)_4][ClO_4]_2$ (5)

We could at best obtain poor quality crystals for $[(L^1)_2Co^{III}_2(CH_3)_4][ClO_4]_2$ (**5**), which could only be refined to a *R* factor of 16.5. Nevertheless, the metal–ligand coordination geometry and associated metrical parameters could be determined, with certainty. A perspective view of the cationic part of **5** is displayed in Figure 5. The asymmetric unit consists of two crystallographically independent $[(L^1)_2Co^{III}_2(CH_3)_4]^{2+}$ cations and four perchlorate anions. Two cobalt centers in each dimer are related by inversion symmetry. The structutre reveals bidentate bridging coordination mode of L^1, which is exactly similar to that observed for complex **2**.[14] Each Co^{III} center is terminally coordinated by two L^1 ligands, each acting as bidentate with pyrazole and pyridine nitrogen donors. The fifth and sixth coordination sites are occupied with two methyl carbon donors. Notably, the complex has four Co–C bonds. This complex is isostructural with complex **2** where methyl groups have replaced the position of bridging acetate anions. Each Co^{III} center therfore assumes a pseudooctahedral CoN_4C_2 coordination geometry (Table 1). The angles between trans atoms at the metal center are in the range

164.8(5)°[162.5(4)°]–172.6(5)°[174.7(5)°]. The cis angles, however, span wide ranges 75.5(6)°[76.0(4)]–102.1(4)°[105.2(4)°]. As in complex **4** here also gross distortions from octahedral geometry are evident. Notably, the angle between the two bidentate 3-(2-pyridyl)pyrazole units in two L^1 is 89.1°(89.9°) which is greater than that in monomers. Average Co–N_{py} (py = pyridine) bond lengths 2.169(12) Å[2.143(11) Å] are slightly longer than average Co–N_{pyrz} (pyrz = pyrazole) bond lengths 2.116(14) Å[2.165(11) Å]. Comparison of the trends in metal–ligand bond lengths reveals that the ligand L^1 coordinates to metal ions more strongly when it acts in a teradentate mononucleating mode [complexes **4** and **6** (see below)] than in a bridging bidentate mode as in complexes **2** and **5**.

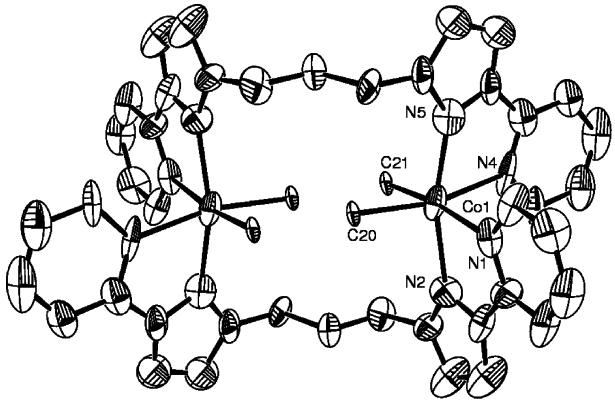

Figure 5. View of the cation $[(L^1)_2Co_2^{III}(CH_3)_4]^+$ in complex $[(L^1)_2Co_2^{III}(CH_3)_4][ClO_4]_2$ (**5**) showing the atom numbering scheme. All hydrogen atoms are excluded for clarity. Symmetry code: $-x$, $-y$, $-z + 1$ and $-x + 1$, $-y$, $-z + 1$.

Structural Description of $[(L^1)Co^{III}(CH_3)_2][BPh_4]$ (6)

A perspective view of the cation of complex **6** is displayed in Figure S6 (Supporting Information). To our surprise, the structural analysis revealed that this complex is closely similar to complex **4**. Metric parameters, however, are slightly different than that observed for complex **4** (Table 1). As that in complexes **4** and **5**, in complex **6** gross distortions from octahedral geometry around Co^{III} are observed. Notably, the Co–C bond lengths are comparatively shorter [1.964(4) and 1.968(4) Å] than that in complex **4**. The angle between the two CoN_2 planes provided by bidentate 3-(2-pyridyl)pyrazole units is 65.9°, which is less than that observed in complex **4** (see above). This implies that in complex **6** the ligand L^1 is more symmetrically coordinated than that in complex **4**, which could be the reason for shorter Co–C bond length in **6**.

Rationalization of the Formation of Co^{III}–$(CH_3)_2$ Complexes and Ligand Flexibility-Driven Mononuclear/Dinuclear Transformation

The formation of the dimethyl–cobalt(III) complexes [monomeric "$Co^{III}(CH_3)_2$" (**4** and **6**) and dimeric "$Co^{III}_2(CH_3)_4$" **5**] due to the reduction of the Co^{III} center(s) in **1** and **2** to the Co^{I} by excess $NaBH_4$ and subsequent reaction of "$Co^{I}(L^1)$" with CH_3I implies that the plausible intermediate "Co^{III}–CH_3" is further reduced to a nucleophilic intermediate "Co^{I}–CH_3",[19e,20] for further reactions with excess CH_3I. The intermediate nucleophilic species "Co^{I}–CH_3" is generated in situ due to the stabilization of such a species as a result of coordination by the bidentate pyridylpyrazile unit present in the ligand L^1 (see below).

The CV bevavior of monomeric dimethyl-cobalt(III) complexes **4** and **6** (see above) reveal two successive irreversible reductive responses: –1.46 V and –1.68 V (**4**) and –1.49 V and –1.73 (**6**) (see above). Comparison of the potential (V vs. SCE) of the Co^{II}–Co^{I} redox process for the monomeric $[Co^{II}(L^1)(H_2O)_2][ClO_4]_2$ (**1**) (–0.96) and dimeric $[Co^{II}_2(L^1)_2(\mu\text{-}O_2CCH_3)_2][BPh_4]_2$ (**2**) (–1.46) cobalt(II) complexes reveals that the $E_{1/2}$ value is more negavive when the Co^{II} center is anion-bound than when it is solvent-bound. Thus, considering the trend in the reduction potential of the Co^{II}–Co^{I} redox process for complex **1** at one hand and complexes **4** (–1.68) and **6** (–1.73) at the other, it is reasonable to assume that the second reduction product for complexes **4** and **6** during electrochemical reduction will be a species like "Co^{I}–CH_3". This justifies our contention that the formation of the dimethyl–cobalt(III) complexes **4**–**6** must have occurred due to the reaction of excess CH_3I with a "Co^{I}–CH_3" species. Unfortunately, the reaction between Co^{I} species [generated due to coulometric reduction of complex **1** in CH_3CN; change of color: from light pink to greenish-blue; *n* (number of electron-transfer) = 0.91] and CH_3I to identify/isolate a mononuclear cobalt(III)-monoalkylated complex did not suceed. In fact, decomposition of the reaction mixture occurred, as judged by redox and spectral studies of such soluitions.

Now we provide a rationale for the formation of the dimeric complex **5** from the monomeric complex **1**. We believe that on reduction both the monomeric (complex **1**) and the dimeric (complex **2**) precursor Co^{II} complexes led to the formation of a distorted tetrahedral monomeric "$[Co^{I}(L^1)]^+$" reactive intermediate species in solution. Given the well-documented weak-field nature of pyridylpyrazole-based ligands[10,11] the distorted tetrahedral over other possible square-planar geometry of cobalt(I) species seems to be more probable. Moreover, the formation of exclusively *cis*-dimethyl products (complexes **4**–**6**) suggests that the reactive intermediate species "$[Co^{I}(L^1)]^+$" has distorted tetrahedral geometry. We believe that in both cases the alkylation reaction takes place via a common monomeric "$[Co^{I}(L^1)]^+$" reactive intermediate. We discard the possibility of the formation of any dimeric intermediate species because in such a situation the metal sites will be sterically hindered for the subsequent alkylation reaction. The $[(L^1)Co^{I}]^+$ intermediate species undergo oxidative methyl addition reaction to yield the monomeric dialkylated complex "$[(L^1)Co^{III}(CH_3)_2]^+$". The alkylation reaction is expected to be very fast, this explains why the kinetically driven product "$[(L^1)Co^{III}(CH_3)_2]^+$" is formed instantly. Hence the formation of the monomeric complex **6** from dimeric cobalt(II) complex **2** is understandable.

Now we pay our attention to the formation of the dimeric tetraalkylated complex $[(L^1)_2Co^{III}_2(CH_3)_4][ClO_4]_2$ (**5**) from

the monomeric precursor complex $[(L^1)Co^{II}(H_2O)_2][ClO_4]_2$ (**1**). A close examination of the crystal structures of monomers **4** and **6** reveals the existence of angular strain in the propylene spacer part of L^1 which gets releaved on dimerization (Table 2). The monomeric complex $[(L^1)Co^{III}(CH_3)_2][ClO_4]$ (**4**), formed from $[(L^1)Co^{II}(H_2O)_2][ClO_4]_2$ (**1**), undergoes a rearrangement in a polar medium through the assistance of solvent molecules to afford a thermodynamically more favored dimeric product $[(L^1)_2Co^{III}_2(CH_3)_4][ClO_4]_2$ (**5**). Comparison of angular strain within the propylene spacer part of L^1 (Table 2) reveals that for complexes with Co^{II} state (complexes **1** and **2**) the strain decreases. Anticipating a similar trend it is expected that in situ generated intermediate "$[(L^1)Co^{I}]^{+}$" species will have a minimum strain. This structural parameter strengthens our contention that the reactive Co^{I} intermediate species is a monomer. Finally, we consider the observed differential yield of the monomeric (complexes **4** and **6** from complexes **1** and **2**, respectively) to the dimeric (complex **5** from complex **1**) dialkyl complexes, when intermediate species is expected to be the same. It is worth noting here the fact that the complexes **1** and **2** differ only in the nature of the counteranion. The former complex has more polar ClO_4^- counterion, which makes it and the product formed from it to be more soluble in a polar medium. The latter complex has bulky and hydrophobic BPh_4^- counterion which makes it and its product more soluble in a nonpolar medium. Due to expected higher solubility of $[(L^1)Co^{III}(CH_3)_2][BPh_4]$ (**6**), the bulk of the compound was extracted into the CH_2Cl_2 layer and hence we could not isolate any dimeric complex from the aqueous phase as in the case of complex **1**. However, in the case of the ClO_4^- salt a large amount of monomeric complex $[(L^1)Co^{III}(CH_3)_2][ClO_4]$ (**4**) remained in the aqueous phase, which eventually rearranged to yield the dimeric complex $[(L^1)_2Co^{III}_2(CH_3)_2][ClO_4]_2$ (**5**) in good yield.

Table 2. Metric parameters associated with propylene spacer of L^1 in the complexes $[(L^1)Co^{II}(H_2O)_2][ClO_4]_2$ (**1**), $[(L^1)_2Co^{II}_2(\mu\text{-}O_2CMe)_2][BPh_4]_2$ (**2**), $[(L^1)Co^{III}(CH_3)_2][ClO_4]$ (**4**), $[(L^1)_2Co^{III}_2(CH_3)_4][ClO_4]_2$ (**5**), and $[(L^1)Co^{III}(CH_3)_2][BPh_4]$ (**6**).

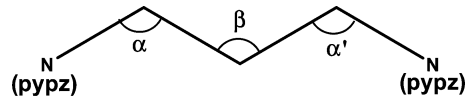

L^1

Compound	α	β	α'
1[a]	113.2°	115.0°	112.8°
2[a]	110.7°	111.4°	111.9°
4	116.2°	118.8°	110.5°
5	108.2°	109.5°	108.2°
	(110.7°)	(114.6°)	(110.4°)
6	116.0°	117.7°	111.6°

[a] Ref.[14].

Concluding Remarks

Using a pyridylpyrazole-based conformationally flexible potentially tetradentate N_4-chelating ligand in the current study chemical/electrochemical generation of Co^{I} and Ni^{I} species has been achieved. It is due to interplay between electronic and stereochemical flexibility of the chosen ligand.

Coulometrically generated Ni^{I} species has been characterized by its absorption and EPR spectroscopic data. Reactions of chemically generated Co^{I} species with CH_3I afforded isolation and structural characterization of monomeric and dimeric dimethyl-Co^{III} complexes. To the best of our knowledge, this is the first example of structurally characterized $Co^{III}(CH_3)_2$ complexes supported by nonmacrocyclic, conformationally flexible pyridylpyrazole-based ligand. Further reactivity studies of Ni^{I} species are underway.

Experimental Section

General: All chemicals were obtained from commercial sources and used as received. Solvents were purified/dried following standard procedures. The ligand L^1 was synthesized following a reported procedure.[15] Tetra-*n*-butylammonium perchlorate (TBAP) was prepared/purified as before.[16]

Syntheses: The complexes $[(L^1)Co^{II}(H_2O)_2][ClO_4]_2$ (**1**), $[(L^1)_2Co^{II}_2(\mu\text{-}O_2CCH_3)_2][BPh_4]_2$ (**2**), and $[(L^1)Ni^{II}(CH_3CN)_2][BPh_4]_2$ (**3**) were obtained as described previously.[14]

Chemical Reduction of Co^{II} Complexes: The cobalt(II) complexes **1** and **2** were reduced chemically by a similar methodology. 1–2 mM solutions of the complexes were purged with N_2 gas (Schlenk-line technique) for 30 min under ice-cold conditions. Three equiv. of powdered $NaBH_4$ were then quickly added to such solutions, under magnetic stirring. Immediately the color of the solutions changed from light pink to greenish blue in the case of complex **1** and from pink to bright green for **2**. Similar color change was also observed during coulometric reduction (see above). Electrochemically generated CH_3CN solutions (298 K) of Co^{I} species were characterized by UV/Vis spectra (the accuracy of the ε values was reasonable, given the instability of the generated solutions): λ (ε, $M^{-1}cm^{-1}$) = 400 (sh) (850), 656 (1000), 895 (240) nm.

Preparation of $[(L^1)Co^{III}(CH_3)_2][ClO_4]$ (4) and $[(L^1)_2Co^{III}_2(CH_3)_4][ClO_4]_2$ (5): Nitrogen gas was bubbled for 30 min through an ice-cold light pink solution of $[(L^1)Co^{II}(H_2O)_2][ClO_4]_2$ (0.100 g, 0.16 mmol) in dry CH_3OH (15 mL). Then powdered $NaBH_4$ (0.020 g, 0.48 mmol) was added with stirring whereupon a change in color of the solution to greenish blue was observed. After 10 min of stirring N_2-purged solution of CH_3I (0.070 g, 0.48 mmol) in dry CH_3OH (6 mL) was added in a dropwise manner. The reaction mixture was allowed to stir for a further 10 min and a color change from greenish blue to orange was observed. After 1 h the reaction was quenched by the addition of water (30 mL) and the resulting mixture was extracted with dichloromethane until the aqueous layer became almost colorless (see below). Organic layer was dried with anhydrous Na_2SO_4. Diffusion of *n*-hexane to this solution resulted in the formation of orange block-shaped single-crystals, suitable for X-ray crystallography (yield 0.025 g, ca. 33%). $C_{21}H_{24}ClCoN_6O_4$ (518.84) (**4**): calcd. C 48.58, H 4.63, N 16.19; found C 48.60, H 4.60, N 16.42. ^1H NMR (CD_3CN; 400 MHz; 298 K): δ = 8.18 (d, J_{HH} = 5.12 Hz, 1 H, H^6 of py), 7.98 (m, 6 H, $H^{3,4}$ of pyridine ring; $H^{4'}$ or $H^{5'}$ of pyrazole ring), 7.62 (d, J_{HH} = 5.12 Hz, 1 H, H^6 of pyridine ring), 7.37 (m, 2 H, H^5 of pyridine ring), 7.14 (m, 2 H, $H^{5'}$ or $H^{4'}$ of pyrazole ring), 0.88 (s, 3H of CH_3), 0.68 (s, 3H of CH_3) ppm. UV/Vis (in CH_2Cl_2): λ (ε, $M^{-1}cm^{-1}$) = 285 (5480), 392 (790), 475 (420) nm.

The above-mentioned aqueous layer was kept for slow evaporation. After 15 d pink needle-like crystals, suitable for crystallographic

analysis, were obtained (yield 0.038 g, ca. 45%). $C_{42}H_{48}Cl_2Co_2N_{12}O_8$ (1037.68) (**5**): calcd. C 48.58, H 4.63, N 16.19; found C 48.50, H 4.68, N 16.35.

Preparation of $[(L^1)Co^{III}(CH_3)_2][BPh_4]$ (6): The complex was prepared using the same procedure as for **4**; however, $[(L^1)_2Co^{II}_2(\mu\text{-}O_2CCH_3)_2][BPh_4]_2$ (0.100 g, 0.066 mmol) in dry CH_3OH (15 mL), $NaBH_4$ (0.016 g, 0.40 mmol), and CH_3I (0.56 g, 0.40 mmol) in dry CH_3OH (8 mL) were used. The organic layer was dried with anhydrous Na_2SO_4. Diffusion of petroleum ether into this solution resulted in the formation of orange block-shaped single-crystals, suitable for X-ray crystallography (yield 0.025 g, ca. 50%). $C_{45}H_{44}BCoN_6$ (738.60) (**6**): calcd. C 73.11, H 5.96, N 11.37; found C 73.05, H 5.80, N 11.28. ^1H NMR (CD_3CN; 400 MHz; 25 °C): δ = 8.20 (d, J_{HH} = 5.88 Hz, 1 H, H^6 of pyridine ring), 8.00, 7.89 (two groups of multiplet, 6 H, $H^{3,4}$ of pyrazole ring; $H^{4'}$ or $H^{5'}$ of pyrazole ring), 7.63 (d, J_{HH} = 5.36 Hz, 1 H, H^6 of pyridine ring), 7.37 (m, 2 H, H^5 of pyridine ring), 7.26 (m, 8 H, Ha of BPh_4), 7.11 (d, 2 H, $H^{5'}$ or $H^{4'}$ of pyrazole ring), 6.97 (t, J_{HH} = 7.4 Hz, 8 H, Hb of BPh_4), 6.82 (t, J_{HH} = 7.2 Hz, 4 H, Hc of BPh_4) 0.91 (s, 3H of CH_3), 0.69 (s, 3H of CH_3) ppm. UV/Vis (CH_2Cl_2): λ (ε, $M^{-1}cm^{-1}$) = 280 (5520), 398 (815), 478 (428) nm.

Chemical Reduction of the Ni^{II} Complex: Under an inert atmosphere (Schlenk-line technique) 1–2 mM solutions of $[(L^1)Ni^{II}(CH_3CN)_2][BPh_4]_2$ in CH_3CN were prepared and shaken with concentrated aqueous solution of $NaBH_4$. After a while a deep purple color developed in the organic phase, which was separated by using a cannula (a similar color change was observed during electrochemical reduction). Absorption spectrum (CH_3CN at 298 K; the accuracy of the ε values are reasonable, given the instability of generated solutions): λ (ε, $M^{-1}cm^{-1}$) = 383 (850), 537 (1230) and 901 (270) nm. X-band EPR spectra (in CH_3CN at 120 K): $g_{\|}$ = 2.261 and $g_{\perp}$ = 2.058. Chemically reduced solutions display similar UV/Vis and EPR data.

Physical Measurements: Elemental analyses were obtained using Thermo Quest EA1110 CHNS-O, Italy. Electronic spectra were recorded using Agilent 8453 diode-array spectrophotometer. ^1H NMR spectral measurements were performed on a JEOL-JNM-LA-400 FT (400 MHz) NMR spectrometer. X-band EPR spectra were recorded on a Bruker EMX 1444 EPR spectrometer operating at 9.455 GHz (fitted with a quartz Dewar for measurements at 120 K). The EPR spectra were calibrated with diphenylpicrylhydrazyl, DPPH (g = 2.0037).

Electrochemistry: Cyclic voltammograms were recorded at 298 K on PAR model 370 electrochemistry system, consisting of a model 174A polarographic analyzer, and a model 175 universal programmer. A standard three-electrode cell was employed with a Beckman M-39273 Pt-inlay working electrode, a platinum-wire auxiliary electrode, and a saturated calomel electrode (SCE) as reference; no corrections were made for junction potentials. The solutions were ca. 1.0 mM in complex and 0.1 M in supporting electrolyte, TBAP. Details of cell configuration and criterion for reversibility are as reported previously.[16] For constant-potential electrolysis (coulometry), a platinum wire-gauze was used as the working electrode. The value of n (number of electrons consumed per mol of complex) was an average of three independent measurements.

Crystallography: Diffraction intensities were collected on a Bruker SMART APEX CCD diffractometer, with graphite-monochromated Mo-K_α (λ = 0.71069 Å) radiation at 298(2) K. For data reduction the Saint Plus program from Bruker was used. Data were corrected for absorption and Lorentz and polarization effects. The structures were solved with SIR-97 and refined with the SHELXL-97 package incorporated in WinGX 1.64 crystallographic collective package.[23] Anisotropic refinements were performed by full-matrix least-squares procedure on F^2. The positions of the hydrogen atoms were calculated assuming ideal geometries, but not refined. The dataset of **4** was

Table 3. Data collection and structure refinement parameters for $[(L^1)Co^{III}(CH_3)_2][ClO_4]$ (**4**), $[(L^1)_2Co^{III}_2(CH_3)_4][ClO_4]_2$ (**5**), and $[(L^1)Co^{III}(CH_3)_2][BPh_4]$ (**6**).

	4	**5**	**6**
Molecular formula	$C_{21}H_{24}ClCoN_6O_4$	$C_{42}H_{48}Cl_2Co_2N_{12}O_8$	$C_{45}H_{44}BCoN_6$
M_r	518.84	1037.68	738.60
Temperature [K]	298(2)	298(2)	298(2)
Radiation used, λ [Å]	Mo-K_α (0.71069)	Mo-K_α (0.71069)	Mo-K_α (0.71069)
Crystal system	monoclinic	triclinic	monoclinic
Space group	$I2/a$ (no. 15)	$P\bar{1}$ (no. 2)	$P2_1/n$ (no. 14)
a [Å]	19.833(5)	13.154(5)	15.378(5)
b [Å]	11.772(5)	13.777(5)	12.548(5)
c [Å]	23.077(5)	13.909(5)	19.690(5)
α [°]	90.000	64.847(5)	90.000
β [°]	109.628(5)	89.594(5)	92.802(5)
γ [°]	90.000	87.604(5)	90.000
V [Å^3]	5075(3)	2279.5(15)	3795(2)
Z	8	2	4
D_c [g cm^{-3}]	1.358	1.512	1.293
μ [mm^{-1}]	0.818	0.911	0.493
F(000)	2144	1072	1552
Crystal size [mm]	0.20 × 0.10 × 0.10	0.10 × 0.05 × 0.05	0.20 × 0.10 × 0.10
Unique reflections	6234	9538	9343
R_{int}	0.1461	0.1311	0.1717
Observed reflections [$I > 2\sigma(I)$]	2017	2811	3725
Refined parameters	298	587	478
R[a] (R_w)[b]	0.0855 (0.2082)	0.1653 (0.3163)	0.0770 (0.1282)
R[a] (R_w)[b] (all data)	0.2038 (0.2321)	0.3611 (0.3933)	0.2038 (0.1658)
Goodness-of-fit on F^2	1.021	0.989	1.002
Largest difference in peak and hole [e Å^{-3}]	0.503, –0.437	1.042, –0.623	0.518, –0.595

[a] $R(F) = \Sigma(||F_o| - |F_c||)/\Sigma|F_o|$. [b] $R_w(F^2) = \{\Sigma[w(|F_o|^2 - |F_c|^2)^2]/\Sigma[w(|F_o|^2)^2]\}^{1/2}$.

treated with the SQUEEZE filter of PLATON[24] due to the presence of severely disordered solvent molecule(s) (probably dichloromethane), which could not be modeled satisfactorily. PLATON estimated the electron count to be 201 electron/cell in a volume of 730 Å^3, out of a unit volume of 5075 Å^3 (14%). For complex **5** the final *R* values are quite high. This may be due to the poor quality of crystal chosen for data collection, and poor dataset obtained. Unfortunately, we could not grow single crystals of **5** that were any better than the one used for the present study, as they were the best we could have. Pertinent crystallographic parameters are summarized in Table 3.

CCDC-716865 (for **4**), -716866 (for **5**) and -716867 (for **6**) contain the supplementary crystallographic data for this paper. These data can be obtained free of charge from the Cambridge Crystallographic Data Center via www.ccdc.cam.ac.uk/data_request/cif.

Supporting Information (see also the footnote on the first page of this article): UV/Vis and ^{1}H NMR spectra of **4**. ^{1}H NMR spectrum and X-ray structure of **6**, cyclic voltammograms of **4** and **6**.

Acknowledgments

Financial assistance received from the Department of Science and Technology (DST), Government of India is gratefully acknowledged. H. M. gratefully acknowledges University Grants Commission (UGC), New Delhi for a Senior Research Fellowship. V. M. sincerely thanks Dr. D. Mandal of our Department for his help in the syntheses of alkyl-Co^{III} complexes. R. M. sincerely thanks the DST for the award of JC Bose fellowship. We thank Atasi Mukherjee for her help in electrochemical experiments.

[1] P. Comba, *Coord. Chem. Rev.* **1993**, *123*, 1.
[2] M. Valente, C. Freire, B. de Castro, *J. Chem. Soc., Dalton Trans.* **1998**, 1557.
[3] P. V. Bernhardt, G. A. Lawrence, in: *Comprehensive Coordination Chemistry-II: From Biology to Nanotechnology* (Eds.: J. A. McCleverty, T. J. Meyer), D. E. Fenton, Amsterdam, Elsevier, **2004**, vol. 6, p. 1.
[4] F. Meyer, H. Kozlowski, in: *Comprehensive Coordination Chemistry, II: From Biology to Nanotechnology* (Eds.: J. A. McCleverty, T. J. Meyer), D. E. Fenton, Amsterdam, Elsevier, **2004**, vol. 6, p. 247.
[5] K. Nag, A. Chakravorty, *Coord. Chem. Rev.* **1980**, *33*, 87.
[6] A. G. Lappin, A. McAuley, *Adv. Inorg. Chem.* **1988**, *32*, 241.
[7] W. R. McWhinnie, J. D. Miller, *Adv. Inorg. Chem. Radiochem.* **1969**, *12*, 135.
[8] L. A. Summers, *Adv. Heterocycl. Chem.* **1984**, *35*, 281.
[9] E. C. Constable, *Adv. Inorg. Chem. Radiochem.* **1986**, *30*, 69.
[10] R. Mukherjee, *Coord. Chem. Rev.* **2000**, *203*, 151 and references cited therein.
[11] a) S. Mahapatra, N. Gupta, R. Mukherjee, *J. Chem. Soc., Dalton Trans.* **1991**, 2911; b) S. Mahapatra, D. Bhuniya, R. Mukherjee, *Polyhedron* **1992**, *11*, 2045; c) S. Mahapatra, R. Mukherjee, *J. Chem. Soc., Dalton Trans.* **1992**, 2337; d) S. Mahapatra, R. Mukherjee, *Indian J. Chem., Sect. A: Inorg. Bio-inorg. Phys. Theor. Anal. Chem.* **1993**, *32*, 64; e) S. Mahapatra, T. K. Lal, R. Mukherjee, *Polyhedron* **1993**, *12*, 1477.
[12] a) S. Mahapatra, R. Mukherjee, *Polyhedron* **1993**, *12*, 1603; b) S. Mahapatra, R. J. Butcher, R. Mukherjee, *J. Chem. Soc., Dalton Trans.* **1993**, 3723; c) S. Mahapatra, R. J. Butcher, R. Mukherjee, *Indian J. Chem., Sect. A: Inorg. Bio-inorg. Phys. Theor. Anal. Chem.* **2001**, *40*, 973; d) S. Singh, V. Mishra, J. Mukherjee, N. Seethalekshmi, R. Mukherjee, *Dalton Trans.* **2003**, 3392.
[13] a) C. Enachescu, J. Linares, F. Varret, K. E. Codjovi, S. G. Salunke, R. Mukherjee, *Inorg. Chem.* **2004**, *43*, 4880; b) V. Mishra, R. Mukherjee, J. Linares, C. Balde, C. Desplanches, J.-F. Létard, E. Collet, L. Toupet, M. Castro, F. Varret, *Inorg. Chem.* **2008**, *47*, 7577.
[14] V. Mishra, F. Lloret, R. Mukherjee, *Inorg. Chim. Acta* **2006**, *359*, 4053.
[15] K. L. V. Mann, J. C. Jeffery, J. A. McCleverty, M. D. Ward, *J. Chem. Soc., Dalton Trans.* **1998**, 3029.
[16] V. Mishra, V. F. Lloret, R. Mukherjee, *Eur. J. Inorg. Chem.* **2007**, 2161.
[17] a) Y. Lin, S. A. Lang Jr., *J. Heterocycl. Chem.* **1977**, *14*, 345; b) H. Brunner, T. Scheck, *Chem. Ber.* **1992**, *125*, 701; c) A. J. Amoroso, A. M. C. Thompson, J. C. Jeffery, P. L. Jones, J. A. McCleverty, M. D. Ward, *J. Chem. Soc., Chem. Commun.* **1994**, 2751; d) F. Wang, A. W. Schwabacher, *Tetrahedron Lett.* **1999**, *40*, 4779.
[18] M. D. Ward, J. A. McCleverty, J. C. Jeffery, *Coord. Chem. Rev.* **2001**, *222*, 251.
[19] a) G. Mestroni, A. Camus, E. Mestroni, *J. Organomet. Chem.* **1970**, *24*, 775; b) M. Calligaris, *J. Chem. Soc., Dalton Trans.* **1974**, 1628; c) R. Dreos, E. Herlinger, G. Tauzher, S. Vuano, G. Nardin, L. Randaccio, *Organometallics* **1998**, *17*, 2366; d) B. Milani, E. Stabon, E. Zangrando, G. Mestroni, A. Sommazzi, C. Zannoni, *Inorg. Chim. Acta* **2003**, *349*, 209; e) G. Tauzher, R. Dreos, A. Felluga, N. Farsich, G. Nardin, L. Randaccio, *Inorg. Chim. Acta* **2004**, *357*, 177; f) P. Kofod, P. Harris, *Inorg. Chem.* **2004**, *43*, 2680, and references cited therein; g) X. Li, H. Sun, A. Brand, H.-F. Klein, *Inorg. Chim. Acta* **2005**, *358*, 3329; h) A. D. Follett, K. A. McNaab, A. A. Peterson, J. D. Scanlon, C. J. Cramer, K. McNeill, *Inorg. Chem.* **2007**, *46*, 1645.
[20] M. W. Whitman, J. H. Weber, *Inorg. Chim. Acta* **1977**, *23*, 263.
[21] P. J. Toscano, L. G. Marzilli, *Prog. Inorg. Chem.* **1984**, *31*, 105.
[22] a) B. D. Gupta, S. Roy, *Inorg. Chim. Acta* **1988**, *146*, 209; b) B. D. Gupta, K. Qanungo, *J. Organomet. Chem.* **1998**, *557*, 243.
[23] L. J. Farrugia, *WinGX v. 1.64*, *An Integrated Systems of Windows Programs for the Solution, Refinement, and Analysis of Single-Crystal X-ray Diffraction Data*, Department of Chemistry, University of Glasgow, **2003**.
[24] PLATON: A. L. Spek, *J. Appl. Crystallogr.* **2003**, *36*, 7.

Received: March 3, 2009
Published Online: June 3, 2009

